Journal of Advanced Research 43 (2023) 233–245

Contents lists available at ScienceDirect

Journal of Advanced Research

journal homepage: www.elsevier.com/locate/jare

Original Article

Optimized integration of metabolomics and lipidomics reveals brain region-specific changes of oxidative stress and neuroinflammation in type 1 diabetic mice with cognitive decline

Fen Xiong, Kaiyan Gong, Hangying Xu, Yingxin Tu, Jiahui Lu, Yiyang Zhou, Wenting He, Wenqing Li, Chen Li, Liangcai Zhao, Hongchang Gao *, Hong Zheng *

Institute of Metabonomics & Medical NMR, School of Pharmaceutical Sciences, Wenzhou Medical University, Wenzhou 325035, China

HIGHLIGHTS

- Over 4000 metabolite and 6000 lipid features were detected in the mouse brain using the optimized extraction method.
- Lipid disorders are more significant in the frontal cortex than the hippocampus in T1D mice.
- Neuroinflammation is more pronounced in the frontal cortex than the hippocampus in T1D mice.
- Brain region-specific shifts in oxidant stress may cause diabetic cognitive decline.
- The frontal cortex might be a major target brain region of oxidant stress in T1D mice.

GRAPHICAL ABSTRACT

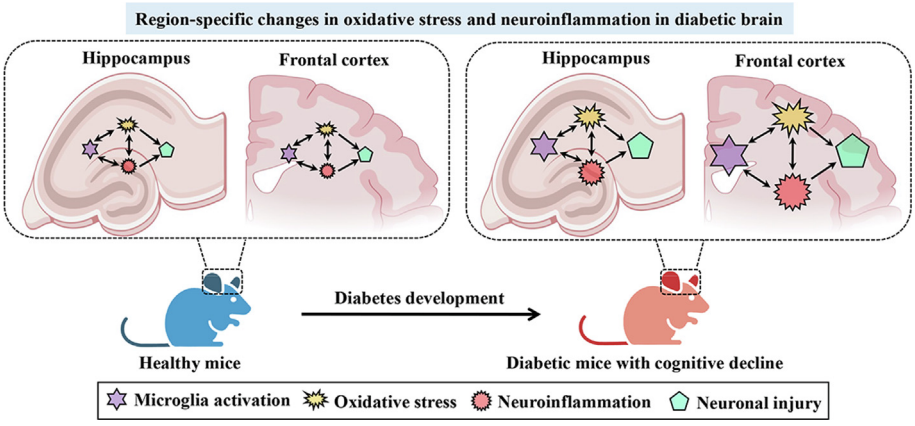

ARTICLE INFO

Article history:
Received 1 November 2021
Revised 8 January 2022
Accepted 19 February 2022
Available online 22 February 2022

Keywords:
Brain
Diabetes
Cognition
Metabolomics
Lipidomics
Neuroinflammation

ABSTRACT

Introduction: Type 1 diabetes (T1D) causes cognitive decline and has been associated with brain metabolic disorders, but its potential molecular mechanisms remain unclear.
Objectives: The purpose of this study was to explore the molecular mechanisms underlying T1D-induced cognitive impairment using metabolomics and lipidomics.
Methods: We developed an optimized integration approach of metabolomics and lipidomics for brain tissue based on UPLC-Q-TOF-MS and analyzed a comprehensive characterization of metabolite and lipid profiles in the hippocampus and frontal cortex of T1D male mice with cognitive decline (T1DCD) and age-matched control (CONT) mice.
Results: The results show that T1DCD mice had brain metabolic disorders in a region-specific manner relative to CONT mice, and the frontal cortex exhibited a higher lipid peroxidation than the hippocampus in T1DCD mice. Based on metabolic changes, we found that microglia was activated under diabetic

Abbreviations: 4-HNE, 4-hydroxynonenal; 8-OHdG, 8-hydroxy-2 deoxyguanosine; CONT, control; CV, coefficient of variation; LC-MS, liquid chromatography mass spectrometry; LOP, lipid peroxidation; NP, number of peaks; OPLS-DA, orthogonal projection to latent structures-discriminant analysis; PCA, principal components analysis; QC, quality control; RT-PC, real-time polymerase chain reaction; STZ, streptozotocin; T1D, type 1 diabetes; T1DCD, type 1 diabetes with cognitive decline; VIP, variable importance in projection.

Peer review under responsibility of Cairo University.

* Corresponding authors.
E-mail addresses: gaohc27@wmu.edu.cn (H. Gao), 123zhenghong321@163.com (H. Zheng).

https://doi.org/10.1016/j.jare.2022.02.011

condition and thereby promoted oxidative stress and neuroinflammation, leading to neuronal injury, and this event was more pronounced in the frontal cortex than the hippocampus.
Conclusion: Our results suggest that brain region-specific shifts in oxidative stress and neuroinflammation may contribute to diabetic cognitive decline, and the frontal cortex could be the more vulnerable brain region than the hippocampus.

Introduction

Type 1 diabetes (T1D) is an autoimmune disease mainly occurring in childhood and adolescent due to pancreatic β cells destruction [1]. The incidence rate of T1D is increasing globally and nearly 1.1 million individuals below 20 years of age are estimated to be diagnosed as T1D in 2019 [2]. Increasing evidence has indicated that T1D contributes to accelerate cognitive impairment [3,4], which might be attributed to vasculopathy [5], neuronal and astrocytic injuries [6], apoptotic neuronal death [7], neuroinflammation [8] and oxidative stress [9]. Besides, our previous studies reported that brain metabolic disorders may be also associated with cognitive decline in both type 2 diabetic *db/db* [10] and T1D [11] mice. It has been well known that metabolic disorders play a crucial role in the onset and development of diseases [12]. Therefore, exploring cerebral metabolic changes in T1D with cognitive decline will facilitate to uncover its pathogeneses and develop potential therapeutic strategies.

Metabolomics aims to detect a comprehensive set of small-molecular metabolites in biological samples using advanced analytical techniques, which has been widely used to explore pathophysiology and identify diagnostic, therapeutic and prognostic biomarkers of diseases [13,14]. Lipidomics, as a branch of metabolomics, has been considered as a complementary approach to systematically analyze all lipids and relevant lipid pathways [15]. Thus, integrated lipidomics and metabolomics contribute to better discover possible molecular mechanisms of diseases. In recent years, an integrated approach of metabolomics and lipidomics has been receiving a great interest in the research field of brain metabolism. Yu et al. developed a parallel metabolomics and lipidomics analytical method to profile region-specific shifts in metabolites and lipids in the brain of mice [16]. This integrated method greatly promotes metabolomics to expose molecular mechanisms underlying brain diseases [16]. However, of note, sample pretreatment is a vital step that affects the quality of omics data [17,18]. Thus, optimizing sample pretreatment method is essential for ensuring the reliability of an integrated study of metabolomics and lipidomics.

In the present study, we aimed to develop an optimized and user-friendly sample pretreatment strategy to obtain high coverage and reproducibility of metabolomics and lipidomics data in the mouse brain based on UPLC-Q-TOF-MS. Subsequently, the developed method was applied to profile the wide changes of metabolites and lipids in the frontal cortex and hippocampus of T1D mice with cognitive decline and to investigate potential molecular mechanisms underlying diabetic cognitive impairment.

Materials and methods

Reagents and materials

Methanol (MeOH), acetonitrile (ACN), isopropanol (IPA), formic acid, and ammonium acetate of HPLC grade were purchased from Thermo Fisher Scientific (Waltham, MA). Chloroform ($CHCl_3$) was analytical grade and purchased from Sinopharm Chemical Reagent Co., Ltd. (Shanghai, China). Streptozotocin (STZ) was purchased from Sigma-Aldrich (St. Louis, MO). Deionized water was purified using a Milli-Q Academic System (Billerica, MA, USA).

Animals

Specific pathogen-free C57BL/6J mice (male, age = 8 weeks) were purchased from the Charles River (Beijing, China) and housed at the Laboratory Animal Center of Wenzhou Medical University (Wenzhou, China) with a stable condition (temperature, 22 ± 1 °C; humidity, 55 ± 5%; light/dark cycle, 12 h/12 h). Mice were given free access to standard mice chow and tap water.

Ethics statement

All experiments involving animals were conducted according to the ethical policies and procedures approved by the Ethics Committee of Wenzhou Medical University, China (Approval no.: xmsq2021-0502).

Streptozotocin-induced diabetic model

After 1 week of acclimation, all mice were randomly divided into the normal control (CONT, n = 9) and diabetic (T1D, n = 9) groups. After 8 h fasting, mice in the T1D group received an intraperitoneal injection with STZ solution prepared in citrate buffer (0.1 M, pH = 4.5) at a dose of 60 mg/kg for 5 consecutive days. Meanwhile, mice in the CONT group were injected with the same volume of citrate buffer. After 5 days of STZ injection, blood glucose level was measured from a tail nick using a handheld glucometer (ACCU-CHEK Active, Mannheim, Germany), and T1D mice were defined when blood glucose level > 11.1 mmol/L. In addition, body weight, daily food intake and daily water intake of mice were also measured in this study.

Morris water maze (MWM) test

In our previous studies, we reported that STZ-induced diabetic rat or mouse model exhibited cognitive dysfunction after 10 weeks of STZ treatment [11,19]. At 11 weeks of STZ injection, therefore, the MWM test was used to assess learning and memory abilities in mice according to our previous study [19]. In this study, to examine the impact of the MWM test on brain metabolic profile, we randomly selected 5 mice in each group for behavioral evaluation and the other 4 mice continued with normal daily feeding. Briefly, the MWM test was carried out in a circular pool (diameter, 110 cm; height, 30 cm) filled with opaque water, and the escape platform (diameter, 7 cm) was submerged below the surface of the water. If mice cannot reach the escape platform within 60 s, during a 4-day training period, mice were guided to arrive at the platform by operator. In the test period, the trained mice were subjected to a 90 s test trial after removing the escape platform. The computer system equipped with an overhead camera was employed to monitor the behavioral changes of mice. Moreover, the percentages of distance and time in goal area and the escape

latency during the training period as well as the platform frequency and the percentages of distance and time in goal area during the test period were calculated with the Viewer-2 software (Biobserve GmbH, Bonn, Germany).

Brain tissue separation and collection

After the MWM test, mice rested for 24 h and were sacrificed by rapid decapitation under isoflurane anaesthesia (5% induction; 2% maintenance) and brain tissue was isolated immediately. The hippocampus and frontal cortex have been commonly considered to serve for cognitive control [20,21]. Thus, the brain was divided into the frontal cortex and hippocampus according to anatomia [22] for further analysis. All brain tissues were frozen in liquid nitrogen rapidly and kept at −80 °C until analysis.

Real-time polymerase chain reaction (RT-PCR) analysis

Total RNA was extracted from the hippocampus and frontal cortex by using TRIZOL reagent (Takara, Shiga-ken. Japan). Then cDNA was reverse-transcribed by PrimeScriptTM RT reagent kit (TaKaRa, RR037A, Tokyo, Japan) and quantified via a Bio-Rad CFX384 (Bio-Rad Laboratories, Inc. CA. USA) and SYBR Green qPCR Master Mix (Takara, Beijing, China). The relative expression level of target genes was quantified with the ΔΔCT method. Each sample was analyzed in triplicate. The primer pairs in this study were listed in Table S1.

Immunohistochemistry

Mice were anesthetized under isoflurane anaesthesia (5% induction; 2% maintenance) and then perfused through the aorta with 0.1 M phosphate-buffered saline (PBS) followed by 4% paraformaldehyde fixative. The brain tissue was dehydrated with a series of graded ethanol, embedded in paraffin and cut into 5 μm sections by using a slicing machine (Leica, Germany). The brain section was incubated with primary antibodies against 8-OHdG (mouse, 1: 100; Abcam, Cambridge, UK), 4-HNE (rabbit, 1: 400; Abcam, Cambridge, UK) and Iba-1 (rabbit, 1: 200; Abcam, Cambridge, UK) overnight at 4 °C, respectively, and then incubated with biotin-conjugated secondary antibodies for 1 h at 37 °C. The brain section was incubated Nissl staining solution (Beyotime Biotechnology, shanghai, Chian) for 1 h at 37 °C. Subsequently, images were acquired with Nikon ECLIPSE Ti microscope and processed by the ImageJ software.

Optimization procedure of metabolomics and lipidomics analyses

In this study, polar and lipid compounds in brain tissue were extracted by using the methanol/water/chloroform (MWC) method. First, we examine the effect of solvent addition sequence on the quality of omics data. Briefly, the frozen brain tissue (10 mg) was weighed into an Eppendorf tube and added with ice-cold methanol/water (v: v, 1: 1) for method 1 or chloroform for method 2. The sample was homogenized completely with a handheld homogenizer, and then added with ice-cold chloroform for method 1 or methanol/water for method 2. For method 3, the brain tissue was weighed into an Eppendorf tube and added with methanol/water/chloroform simultaneously. Subsequently, the mixture was stood on ice for 15 min after vortexing for 15 s, and centrifuged at 10,000*g* for 15 min at 4 °C. Finally, the supernatant was transferred to a new tube, dried under a N_2 stream, and stored at −80 °C until analysis.

Then, the mixture design method was used to optimize solvent addition ratio for maximizing the coverage and reproducibility of omics data under Design-Expert software (Stat ease, Minnesota, USA). In this study, there were two independent variables, methanol/water (X1, 50 %MeOH) and chloroform (X2, $CHCl_3$), and one response variable (Y, the number of reliable peaks). The detailed experimental design was listed in Table S2. Each extraction was carried out in quintuplicate.

UPLC-QTOF/MS analysis

In the MWC extraction, the upper phase containing polar compounds was subjected to metabolomics and the lower phase containing lipid compounds to lipidomics. The dried polar compounds were reconstituted in 100 μL of ACN/water (1: 1, v: v) and the dried lipid compounds were reconstituted in 125 μL of $CHCl_3$/MeOH (1: 1, v: v). Then the mixture was centrifuged for 15 min at 15,000*g* at 4 °C, and the supernatant was collected for LC-MS/MS analysis. Sample analysis was conducted on a SHIMADZU CBM-30A Lite LC system (Shimadzu Corporation, Kyoto, Japan) coupled to an API 6600 Q-TRAP (AB SCIEX, Foster City, CA, USA) mass detector within a 80–1200 *m*/*z* mass range for ESI+ and ESI- models. Polar and lipid compounds separation were separated on a Waters Acquity amide-based HILIC column (2.1 × 100 mm, 1.7 μm) and Phenomenex kinetex C18 column (2.1 × 100 mm, 2.6 μm), respectively. The mobile phase of polar compounds was consisted of 5 mM ammonium acetate and 0.1% formic acid in water (A) and acetonitrile (B) at a flow rate of 0.3 mL·min^{-1}. The gradient elution was as follows: 0–0.5 min, 98% B; 0.5–13 min, 98–40% B; 13–3.1 min, 40–98% B; 13.1–18 min, 98–98% B. The column temperature was set at 35 °C. The injection volume was 2 μL. The collision energy of fragment was 40 V. The mobile phase of lipid compounds with the following conditions: (A) H_2O: MeOH: ACN (3: 1: 1, v: v: v) with 5 mM ammonium acetate, (B) IPA, at a flow rate of 0.3 mL·min^{-1}. Analysis was performed in gradient elution as follows: 0–0.5 min, 25% B; 0.5–1.5 min, 25–40% B; 1.5–3 min, 40–60% B; 3–13 min, 60–98% B; 13–13.1 min, 98–25% B; 13.1–18 min, 25–25% B. The column temperature was controlled at 40 °C. Volume of sample introduced into injector was 1 μL. The collision energy used for the fragmentation was 40 V.

Data preprocessing and analysis

After data acquisition, raw data were converted to mzXML format and subjected to data preprocessing including peak alignment and peak picking using the XC-MS software (XC-MS plus, CA, USA). The main parameters were set as follows: peakwidth = 50, Bw = 0.1, Mzwid = 0.1, Minfrac = 80%. Then, three-dimensional raw datasets including their *m*/*z*, retention time (RT) and peak intensity were exported into Microsoft Excel 2020 (Microsoft Corp., Redmond, WA). In this study, peaks with intensity below 500 were excluded from further analysis. The coefficient of variation (CV, standard deviation/average intensity × 100%) was calculated to indicate data reproducibility by Microsoft Excel 2020, and peaks with CV% >30% were defined as high variability peaks. Therefore, peaks with intensity > 2000 and CV% <30% in positive mode and with intensity > 1000 and CV% <30% in negative mode were selected as reliable peaks for further analysis.

In this study, metabolites were identified via MetDNA2 (http://metdna.zhulab.cn/) and One-MAP (http://www.5omics.com/) based on accurate *m*/*z* value and MS/MS characteristic fragments. We identified 780 and 210 metabolites from MetDNA2 and One-MAP, respectively. Moreover, LipidView software (v1.2, AB Sciex, MA, USA) was used for lipid identification according to accurate mass and MS/MS fragments. Finally, these identified metabolites and lipids were further verified by using the HMDB 4.0 [23].

Prior to univariate and multivariate data analyses, LC-MS raw data were normalized by using Log 10 transformation and Pareto

scaling. Multivariate analysis including principal components analysis (PCA) and orthogonal projection to latent structures-discriminant analysis (OPLS-DA) were conducted by SMICA-P software (v14.0, Umetrics, Umea, Sweden). PCA, an unsupervised model, was used to examine the overview of metabolic pattern changes between CONT and T1DCD mice. OPLS-DA, a supervised model, was performed to further evaluate the metabolic differences between CONT and T1DCD mice in different brain regions and identify important metabolites. A 10-fold cross validation was applied to assess the performance of OPLS-DA, where R^2 and Q^2 were calculated as indicators for goodness of fitness and prediction of the model, respectively. These two parameters close to 1.0 indicate a qualified model. Important metabolites responsible for classification were identified by the variable importance in the projection (VIP) scores of OPLS-DA. Venn diagrams were drawn via an online website (http://bioinformatics.psb.ugent.be/webtools/Venn/index.html). Metabolic pathway analysis was carried out by using Metaboanalyst 5.0 (https://www.metaboanalyst.ca/).

In this study, data are presented as mean ± standard error of the mean (SEM). The difference among three groups was evaluated using one-way ANOVA with pairwise comparison and the difference between two groups was analyzed using two-tailed unpaired Student's *t*-test in SPSS software (IBM SPSS statistics 22). The escape latency during the training period in the MWM test was analyzed by repeated measure analysis in SPSS software. A statistically significant significance was defined when p value < 0.05.

Results

Optimized integration of metabolomics and lipidomics profiling in the brain tissue of mice by UPLC-Q-TOF-MS

In this study, prior to sample extraction, brain tissue was first broken up by using a tissue homogenizer directly in the extraction solvent system. To acquire both metabolomics and lipidomics data from the same sample, a two-phase extraction method composed of methanol/water/chloroform was carried out under LC-MS-based analytical platform (Fig. 1A). The advantage of this method is the simultaneous extraction of both polar and lipid components into two different partitions [24]. In this process, the upper phase (methanol/water layer) containing polar compounds was subjected to metabolomics analysis and the lower phase (chloroform layer) containing lipid compounds to lipidomics analysis, as illustrated in Fig. 1A. In the present study, the extraction procedure was optimized and the number of peaks (NP) and coefficient of variation (CV) were calculated to evaluate the coverage and reproducibility of omics data, respectively. First, we examined the effect of solvent addition sequence on the data quality of metabolomics and lipidomics in the brain tissue of mice, including method 1, adding methanol/water first and then chloroform; method 2, adding chloroform first and then methanol/water; method 3, adding all solvents simultaneously. The results demonstrate that the number of reliable peaks in both positive (NRPP, Fig. 1B) and negative mode (NRPN, Fig. 1C) were significantly higher in method 1 when compared with other two methods using an amide-based HILIC column. There were two reasons for this phenomenon: on the one hand, in method 1, brain tissue was first homogenized in the methanol/water solvent system, which facilitated the extraction of polar metabolites into the polar phase; on the other hand, HILIC is more favorable to analyze polar metabolites in both positive and negative modes [25,26]. Using a C18 column, we found that NRPN was significantly higher in method 1 relative to other two methods (Fig. 1E), which might be due to the fact that polar lipids extracted by method 1 are better detected with negative ionization [27]. However, there was no significant difference in NRPP between method 1 and method 2 (Fig. 1D), indicating that chloroform addition sequence had a lesser impact on the data quality of lipidomics in the brain tissue using a C18 column in positive mode. Additionally, method 3 of all solvents simultaneously was not a suitable extraction strategy for both metabolomics and lipidomics analysis in the brain tissue of mice, which is in agreement with the finding of Wu et al. [28] in fish liver for metabolomics. They also reported that this all-in-one approach can extract macromolecular metabolites, resulting in lower ionization efficiency for other metabolites during LC-MS analysis [28]. Overall, our results reveal that method 1, namely adding methanol/water first and then chloroform, can acquire higher coverage and reproducibility of both metabolomics and lipidomics data in the brain tissue of mice, but whether this method is also applicable to other types of tissues cannot be concluded in the current study.

Of note, different solvent ratios result in different polarities and thereby affect the extraction efficiency of metabolites or lipids. To improve the data quality of metabolomics and lipidomics, therefore, optimizing the ratio of extraction solvent system is of great importance due to metabolite or lipid variations across different tissues [29]. Herein we used mixture design method to optimize the ratio of extraction solvent for metabolomics and lipidomics in the brain tissue of mice by maximizing NRPP and NRPN. The detailed experimental results were listed in Table S3. Moreover, a contour plot showing changes in the number of reliable peaks as a function of 50 %MeOH and $CHCl_3$ was used to determine the optimal extraction method. The results show that the optimal proportions of 50 %MeOH:$CHCl_3$ for analyzing polar and lipid compounds in the mouse brain were 16:4 (Fig. 1F) and 9:11 (Fig. 1G), respectively. Yet, for analyzing both polar and lipid compounds, the optimal proportion of 50 %MeOH:$CHCl_3$ was 9.8:10.2 (Fig. 1H). Using the optimized extraction method, we detected>4000 metabolite and 6000 lipid features simultaneously in the same mouse brain, where 990 metabolites and 1330 lipids were identified via automated MS/MS spectral matching.

Optimized metabolomics and lipidomics analyses reveal brain region-specific shifts of metabolites and lipids in T1DCD mice

Typical T1D symptoms occurred in mice treated with STZ as indicated by significantly higher levels of blood glucose (Figure S1A), daily food intake (Figure S1C) and daily water intake (Figure S1D) but lower body weight (Figure S1B) relative to normal control mice. The MWM test was employed to evaluate the learning and memory abilities of mice. During the training period, the percentages of distance and time in goal area and the escape latency of T1DCD mice were significantly longer than that of CONT mice (Fig. 2A-2C). The swimming trajectories of CONT and T1DCD mice during the test period were illustrated in Fig. 2D and 2E, respectively. Then, we calculated several behavioral indicators and the results reveal that the number of crossings over the original platform location (Fig. 2F), and the percentages of the distance (Fig. 2G) and time (Fig. 2H) in goal area during the test period were significantly reduced in T1DCD mice relative to CONT mice, suggesting impaired learning and memory abilities in T1DCD mice.

To explore potential metabolic mechanisms underlying T1D-associated cognitive decline, the optimized analytical method proposed herein was employed to acquire both metabolomics and lipidomics profiling in the hippocampus and frontal cortex, as two main brain regions involved in cognitive processes [20,21]. First, we observed that quality control (QC) samples were center-clustered in PCA score plots, indicating a good instrumental reproducibility across different analytical runs (Figure S2). Additionally, brain metabolic patterns were not significantly differed in mice with and without the MWM test (Fig. 3A-3D; Figure S3). These results indicate high reliability of metabolomics and lipidomics

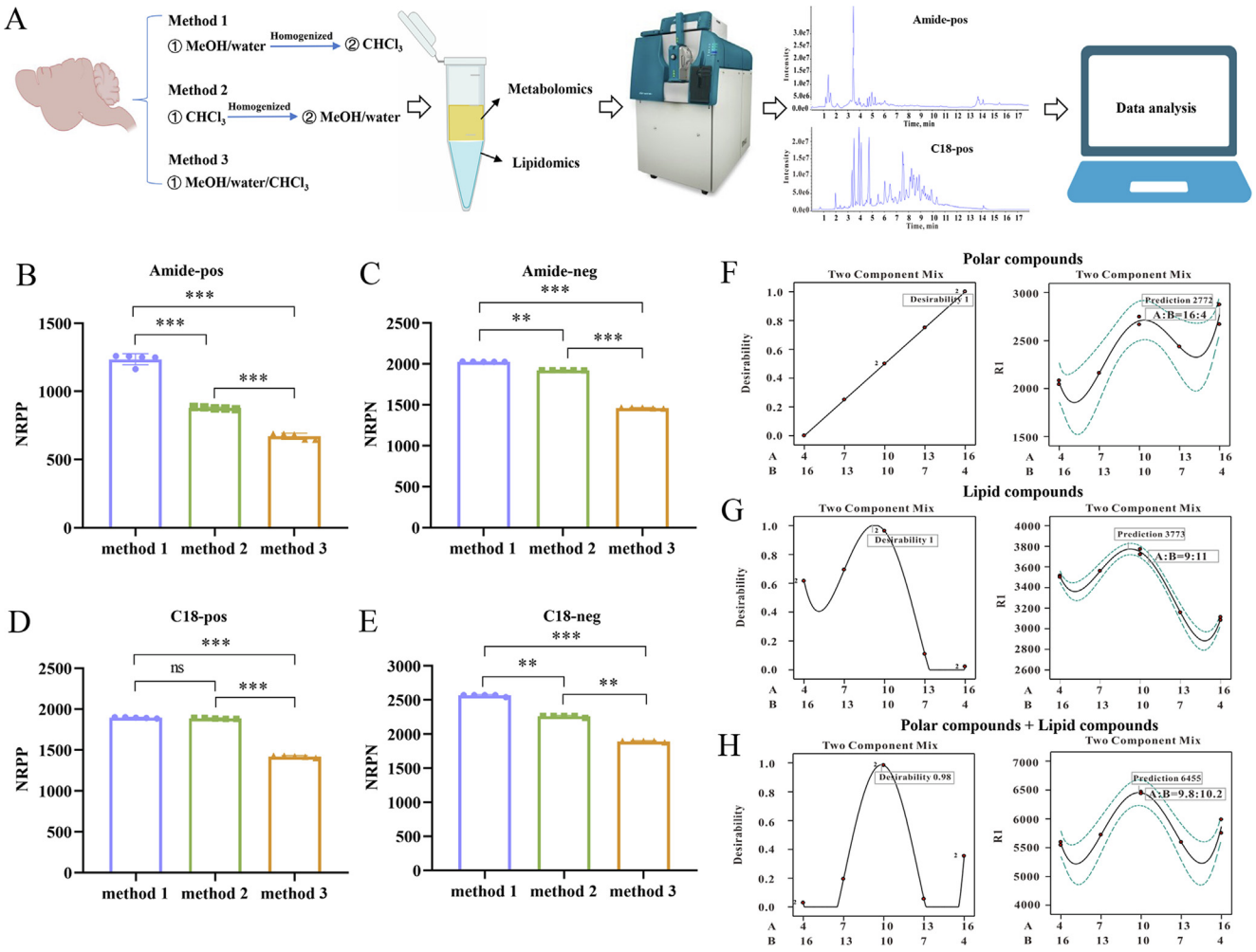

Fig. 1. Integrated analytical method for metabolomics and lipidomics in the mouse brain based on UPLC-Q-TOF-MS. (A) The analytical workflow: a two-phase extraction approach (methanol/water/chloroform) was carried out to extract metabolites in the brain of mice, where the upper phase (methanol/water layer) containing polar compounds was subjected to metabolomics analysis and the lower phase (chloroform layer) containing lipid compounds to lipidomics analysis. (B) The number of reliable peaks (CV% <30%; intensity > 2000) in positive mode (NRPP) using an amide-based HILIC column. (C) The number of reliable peaks (CV% <30%; intensity > 1000) in negative mode (NRPN) using an amide-based HILIC column. (D) The number of reliable peaks (CV% <30%; intensity > 2000) in positive mode (NRPP) using a C18 column. (E) The number of reliable peaks (CV% <30%; intensity > 1000) in negative mode (NRPN) using a C18 column. Mixture design method was used to optimize the ratio of extraction solvent by maximizing NRPP and NRPN, and the contour plots showing changes in NRPP and NRPN (R1) as a function of 50 %MeOH and $CHCl_3$ for analyzing (F) polar compounds, (G) lipid compounds and (H) both polar and lipid compounds in the mouse brain. Data are presented as mean ± standard error of the mean (SEM). The difference among three groups was assessed using one-way ANOVA with pairwise comparison. Significant level: **, $p < 0.01$; ***, $p < 0.001$; ns, $p > 0.05$.

data. The PCA score plots show that clear separations were obtained between CONT and T1DCD mice in the frontal cortex and hippocampus based on both metabolomics and lipidomics data (Fig. 3A-3D; Figure S4), suggesting that cerebral metabolome and lipidome were significantly altered in T1DCD mice. Subsequently, we identified important differentiated metabolites and lipids between CONT and T1DCD mice using multivariate (OPLS-DA, Figure S4) and univariate analyses (T-test, Tables S4-S7). In this study, metabolites or lipids with VIP-value > 1.0 and *p*-value < 0.05 were selected for further analysis, as listed in Tables S4-S7.

Venn diagram analysis shows that there were 11 common features in these two brain regions, while 129 and 124 features were identified as unique features in the frontal cortex and hippocampus, respectively (Fig. 3E). The levels of L-methionine, *N*-acetyl-L-aspartate, citrate, docosanoylcarnitine, L-carnitine, ethanolamine phosphate, and DG(9D5/9D5/0:0)) were significantly decreased, while S-glutathionyl-L-cysteine, (2S,4S)-4-hydroxy-2,3,4,5-tetrahydrodipicolinate (HDT), and D-glucose-6-sulfate were significantly increased in these two brain regions of T1DCD mice when compared with CONT mice as shown in Figure S5. Moreover, the level of PA(16:1/16:0) was found to be higher in the frontal cortex but lower in the hippocampus of T1DCD mice than CONT mice (Figure S5). Interestingly, relative to the frontal cortex, we detected more differentiated polar compounds (81 vs. 34) but lesser lipid compounds (43 vs. 95) in the hippocampus (Fig. 3F). These differentiated features mainly include alcohols, hydroxy acids, amino acids, carboxylic acids, keto acids, organic acids, organonitrogen compounds, purine, pyrimidines, indoles, phospholipids, steroids, glyceride, sphingolipids, and diterpenoids (Fig. 3G–J). Amino acids were detected as the predominant type of polar compounds in both the frontal cortex (32%, Fig. 3G) and hippocampus (26%, Fig. 3H), while glycerophosphoethanolamine and fatty acyls were the predominant types of lipid compounds in the frontal cortex (30%, Fig. 3I) and hippocampus (20%, Fig. 3J), respectively. These results indicate that region-specific metabolic shifts occurred in the brain of T1DCD mice.

Fig. 4 illustrates the biological functions linked to these differentiated metabolites and lipids in the hippocampus and frontal cortex between CONT and T1DCD mice, mainly including oxidative stress, lipid peroxidation, lipid metabolism, neurotransmitters, and

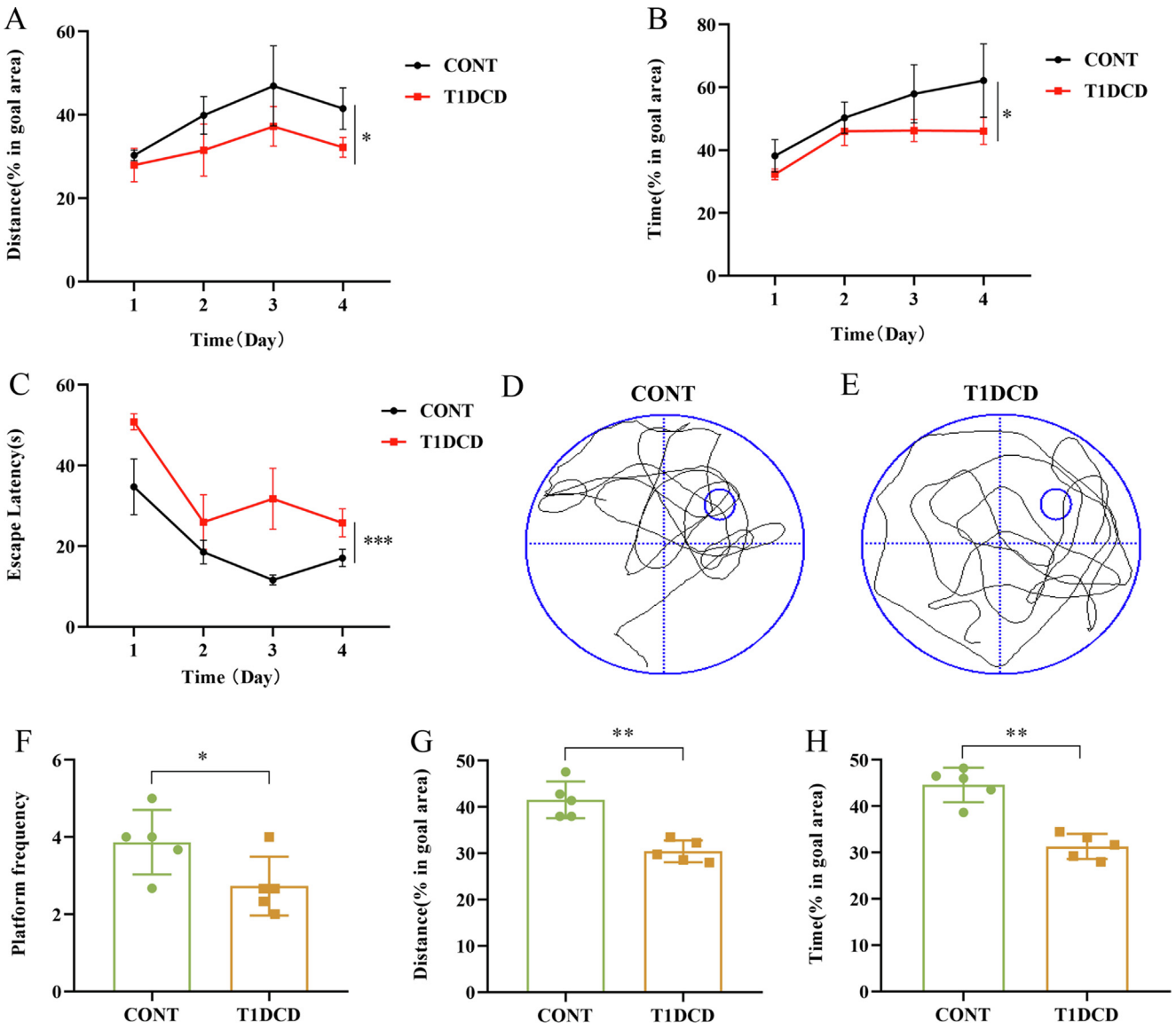

Fig. 2. Impaired learning and memory abilities in type 1 diabetic mice. The Morris water maze test was used to evaluate the learning and memory abilities of mice. The percentages of swimming (A) distance and (B) time in goal area of type 1 diabetic mice with cognitive decline (T1DCD) and age-matched control (CONT) mice during the training period. (C) The escape latency of T1DCD and CONT mice during the training period. The swimming trajectories of (D) CONT and (E) T1DCD mice during the test period. (F) The number of crossings over the original platform location of CONT and T1DCD mice during the test period. The percentages of swimming (G) distance and (H) time in goal area of CONT and T1DCD mice during the test period. (F) The percentage of swimming time in goal area. Data are presented as mean ± standard error of the mean (SEM). The behavioral changes over time during the training period were analyzed by repeated measure ANOVA. The difference between two groups was analyzed using two-tailed unpaired Student's *t*-test. Significant level: *, $p < 0.05$; **, $p < 0.01$.

energy metabolism. Relative to the hippocampus, interestingly, we found that a higher level of oxidative stress occurred in the frontal cortex of T1DCD mice. T1DCD mice had a higher level of S-glutathionyl-L-cysteine as a precursor of glutathione than CONT mice in both brain regions, while the glutathione level was not significantly altered (Fig. 4). However, of note, oxidized glutathione (GSSG), a biomarker of oxidation stress, was detected to be significantly increased only in the frontal cortex of T1DCD mice relative to CONT mice. We found that the levels of proline and arginine, which have been reported to suppress oxidative stress [30,31], were significantly reduced in the frontal cortex of T1DCD mice compared with CONT mice (Fig. 4A), but not in the hippocampus (Fig. 4B). L-methionine as an important intracellular antioxidant [32] was significantly decreased in both brain regions of T1DCD mice relative to CONT mice. Moreover, L-cysteate, a product of methionine metabolism, was significantly reduced only in the hippocampus of T1DCD mice than CONT mice (Fig. 4B).

Reactive oxygen species (ROS) can react with unsaturated fatty acids and then initiate lipid peroxidation [33]. Therefore, higher oxidative stress resulted in higher levels of lipid peroxidation and lipid metabolism disorders in the frontal cortex of T1DCD mice (Fig. 4). The results demonstrate that T1DCD mice had significantly lower levels of docosanoylcarnitine, L-carnitine, and L-acetyl-carnitine in the hippocampus (Fig. 4B) as well as (R)-2-Methylmalate, L-carnitine, and docosanoylcarnitine in the frontal cortex (Fig. 4A) than CONT mice. Docosanoylcarnitine and L-acetyl-carnitine are derived from L-carnitine, which is implicated in fatty acid β-oxidation. Thus, these results indicate that fatty acid oxidation disorders occurred in the hippocampus and frontal cortex of T1DCD mice. Hexadecanamide derived from palmitic acid (C16:0) is a primary fatty acid amide and plays an important role in cellular signaling transduction. In this study, we identified a significantly lower hexadecanamide in the hippocampus of T1DCD mice (Fig. 4B). A total of 10 different glycerophospholipids and

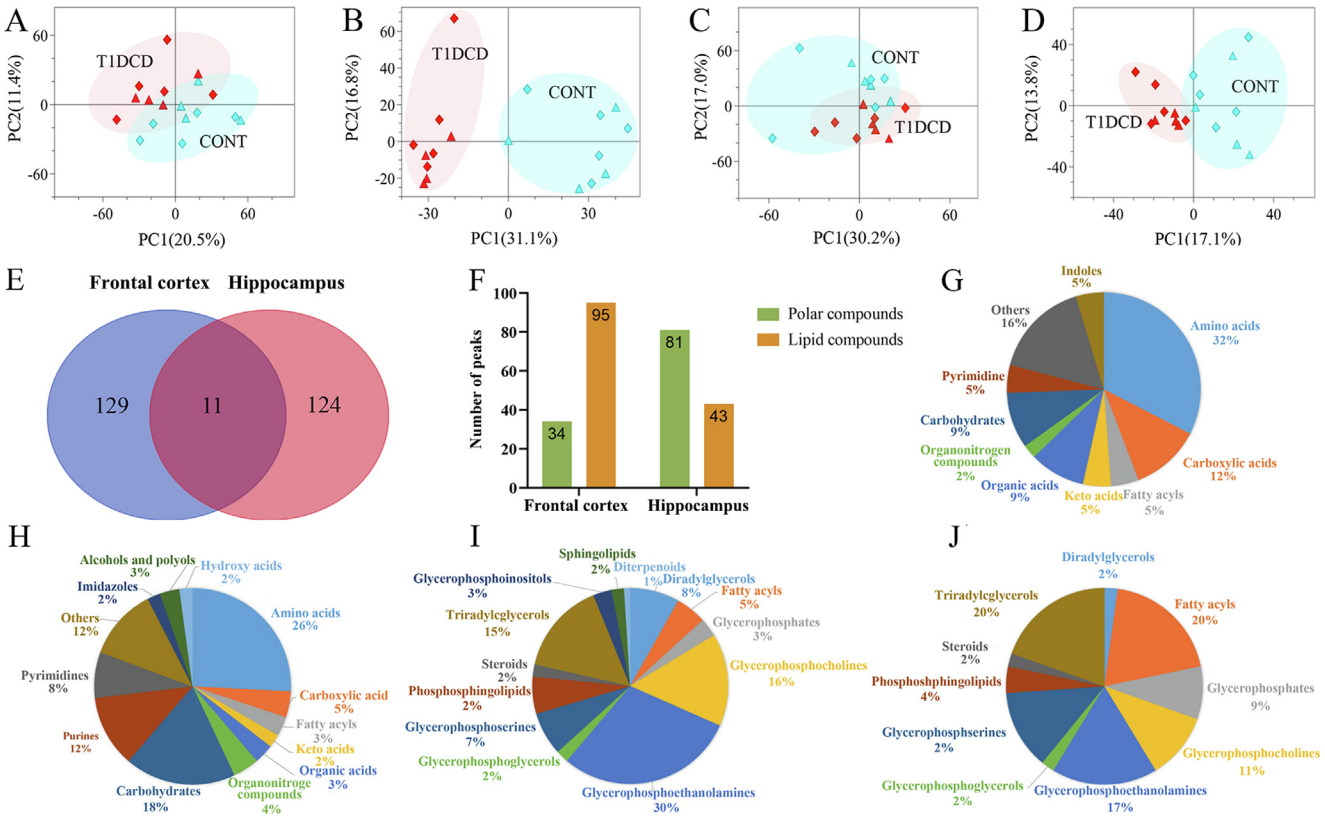

Fig. 3. Brain region-specific changes of metabolites and lipids in type 1 diabetic mice with cognitive decline. Metabolic pattern changes in the (A, B) frontal cortex and (C, D) hippocampus between type 1 diabetic mice with cognitive decline (T1DCD) and age-matched control (CONT) mice were analyzed by PCA based on Amide positive and negative modes, respectively. To examine the impact of the Morris water maze test on brain metabolic profile, we randomly selected 5 mice in each group (rhombus marker) for behavioral evaluation and the other 4 mice (triangle marker) continued with normal daily feeding. (E) Venn diagram showing the common and unique features in the frontal cortex and hippocampus between T1DCD and CONT mice. (F) Histogram showing the number of differentiated polar and lipid compounds in the frontal cortex and hippocampus between CONT and T1DCD mice. The classes of polar compounds in the (G) frontal cortex and (H) hippocampus and lipid compounds in the (I) frontal cortex and (J) hippocampus.

glycerolipids classes were identified, such as phosphatidylcholine (PC), phosphatidylethanolamine (PE), triglyceride (TG), diacylglycerol (DG), phosphatidylserine (PS), phosphatidic acid (PA), glycerophospholipid (PG), lysoPC, phosphatidylinositols (PI), and lysoPE (Fig. 4). Interestingly, the number of differentiated PC (13 vs. 5), PE (26 vs. 5), DG (12 vs. 1), and TG (15 vs. 9) between T1DCD and CONT mice was more in the frontal cortex than the hippocampus. The levels of most PC were significantly decreased in both hippocampus (3/5) and frontal cortex (9/13) of T1DCD mice, which is in agreement with the finding in T1D patients [34]. Compared with CONT mice, the levels of PE were significantly increased in these two brain regions of T1DCD mice. Lower levels of ethanolamine phosphate and CDP-ethanolamine as precursors of PE were detected in T1DCD mice than CONT mice. In the hippocampus, a higher level of TG was observed in T1DCD mice relative to CONT mice. Also, we found that 10/15 of TG were significantly increased in the frontal cortex of T1DCD mice, as shown in Fig. 4A. The levels of most DG (11/12) were significantly increased in the frontal cortex of T1DCD mice compared with CONT mice (Fig. 4A), but not in the hippocampus (Fig. 4B). Relative to CONT mice, the levels of most PS (4/6) were significantly decreased in the frontal cortex of T1DCD mice, but increased in the hippocampus. Besides, we also identified a small number of PA, PG, PI, lsyoPC, and lysoPE were disordered in these two brain regions of T1DCD mice. Disrupted lipid metabolism is intertwined with lipid peroxidation and oxidative stress, and ultimately destroys cellular membrane structure and causes cell apoptosis and necrosis [35,36]. The abnormality of lipid metabolism might be the potential molecular mechanisms underlying T1D-associated cognitive impairment.

Neurotransmitter metabolism was disrupted in both the hippocampus and frontal cortex of T1DCD mice. L-3,4-dihydroxyphenylalanine (L-dopa) as a precursor of dopamine was significantly lower in the hippocampus of T1DCD mice relative to CONT mice (Fig. 4B). *N*-Acetyl-L-aspartate, L-aspartate, *N*-(L-arginion)-succinate, and L-glutamate-5-semialdehyde are implicated in the synthesis of glutamate, an excitatory neurotransmitter [37], but their levels were found to be significantly decreased in the hippocampus of T1DCD mice than CONT mice. L-alanine and taurine as an inhibitory neurotransmitter [38,39] was also significantly reduced in the hippocampus of T1DCD mice. Acetylcholine serves as a neurotransmitter, which is an ester of acetic acid and choline. In this study, relative to CONT mice, the levels of acetylcholine, choline, and phosphorylcholine were significantly increased in the hippocampus of T1DCD mice. In the frontal cortex, the levels of L-phenylalanine, L-tryptophan, and L-tyrosine were significantly reduced in T1DCD mice compared with CONT mice (Fig. 4A). Of note, L-tryptophan and L-tyrosine are considered as the precursors of neurotransmitter 5-hydroxytryptophan and dopamine, respectively. Moreover, *N*-acetyl-L-aspartate, L-glutamyl-5-phosphate, proline, arginine, and 3-sulfino-L-alanine, which are involved in glutamate biosynthesis, were also significantly decreased in the frontal cortex of T1DCD mice (Fig. 4A). We speculate that brain region-specific shifts in neurotransmitter metabolism may facilitate cognitive impairment in T1D mice.

The abnormal energy metabolism is another key metabolic feature related to diabetic cognitive dysfunction. A disruption of the TCA cycle was found in the brain of T1DCD mice relative to CONT mice, as indicated by lower levels of citrate in the hippocampus

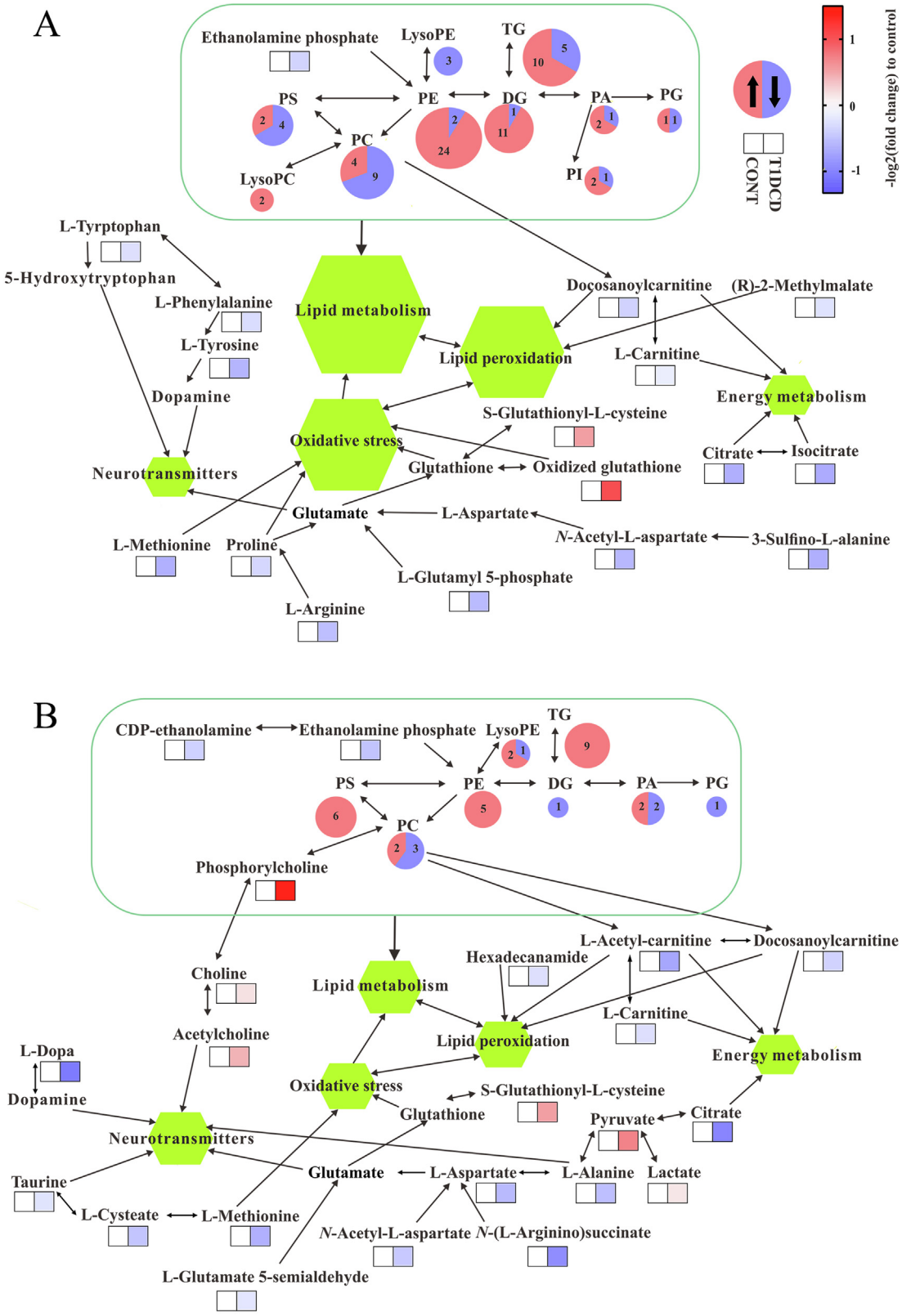

Fig. 4. Brain region-specific metabolic alterations in type 1 diabetic mice with cognitive decline. The changes in metabolites in the (A) frontal cortex and (B) hippocampus between type 1 diabetic mice with cognitive decline (T1DCD) and age-matched control (CONT) mice are illustrated as heatmaps. The color key in the heatmap from red to blue indicates high to low fold changes in metabolite levels in T1DCD mice relative to CONT mice, respectively. The changes in lipids are presented as pie charts. Number in the pie chart indicates the number of differentiated lipids between CONT and T1DCD mice, which is proportional to the pie size. Red or blue color in the pie chart represents high or low lipid level in T1DCD mice relative to CONT mice. The biological functions linked to differentiated metabolites and lipids between CONT and T1DCD mice are presented as green hexagons, mainly including oxidative stress, lipid peroxidation, lipid metabolism, neurotransmitters, and energy metabolism. The size of green hexagon is proportional to the number of metabolites or lipids linked.

(Fig. 4B) as well as citrate and isocitrate in the frontal cortex (Fig. 4A). Moreover, the levels of pyruvate and lactate were significantly increased in the hippocampus of T1DCD mice than CONT mice. Fatty acid β-oxidation is another important energy source in the brain, but herein we found that the levels of two related metabolites, L-carnitine and L-acetyl-carnitine, were significantly reduced in these two brain regions of T1DCD mice relative to CONT mice (Fig. 4).

Nucleotide metabolism plays an essential role in regulating cellular homeostasis including carbohydrate metabolism, nucleotide biosynthesis and signal transduction [40]. In this study, we found that disordered nucleotide metabolism occurred mainly in the hippocampus but not in the frontal cortex of T1DCD mice (Figure S6). Relative to CONT mice, the levels of dGDP, dATP, dUDP, UDP, adenine, xanthosine, guanine, guanosine, inosine, IDP, D-ribose-5-phosphate, cyclic ADP-ribose, and *N*-acetyl-D-glucosamine-1-phosphate were significantly decreased in the hippocampus of T1DCD mice, while 3′-CMP, UDP-glucose, ADP, adenosine, and AIR were significantly increased (Figure S6B). However, in the frontal cortex, we only identified lower levels of cytosine and cytidine in T1DCD mice than CONT mice (Figure S6A). Therefore, our results suggest that brain region-specific disorders in nucleotide metabolism might also be a risk factor for cognitive decline in T1D mice.

Higher oxidative stress status occurred in the frontal cortex than the hippocampus of T1DCD mice

In this study, PCR analysis and immunohistochemical staining were carried out to confirm region-specific changes of oxidative stress in the brain of T1DCD mice (Fig. 5). The results show that the mRNA levels of prooxidants, *Nox2*, *Nox4* and *Aco*, were significantly higher in the frontal cortex (Fig. 5A) of T1DCD mice than CONT mice, while only *Aco* exhibited a statistically significant increase in the hippocampus (Fig. 5C). Relative to CONT mice, T1DCD mice had significantly decreased mRNA levels of antioxidants including *Sod2*, *Nqo1*, *Nrf2* and *Gpx-1* in both the frontal cor-

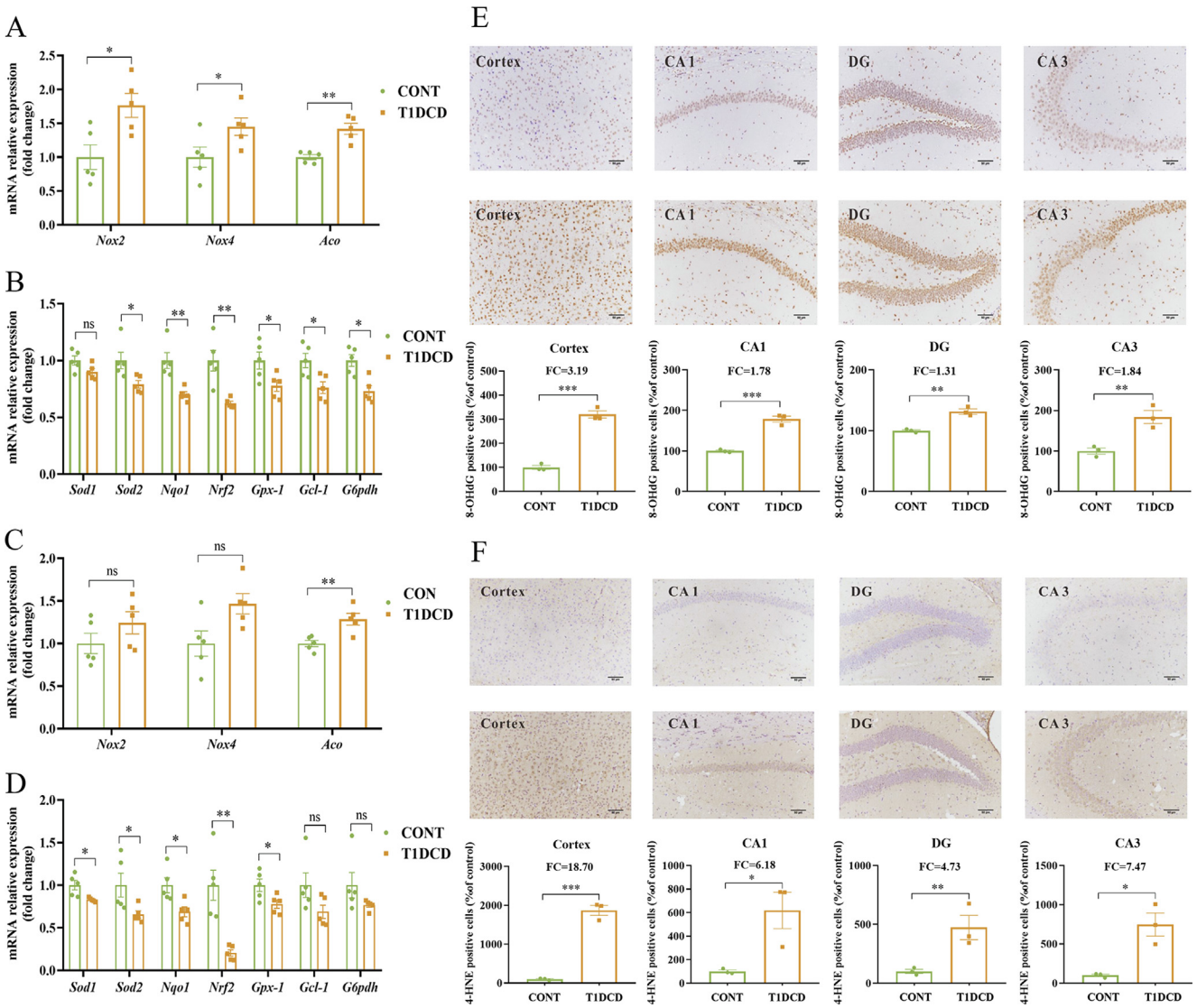

Fig. 5. Brain region-specific changes in oxidative stress in type 1 diabetic mice with cognitive decline. Changes in the mRNA expression levels of (A) antioxidants and (B) prooxidants in the frontal cortex between type 1 diabetic mice with cognitive decline (T1DCD) and age-matched control mice (CONT). Changes in the mRNA expression levels of (C) antioxidants and (D) prooxidants in the hippocampus between T1DCD and CONT mice. (E) Representative immunohistochemical staining of 8-OHdG proteins (brown spots, 200×) and corresponding quantitative results in the frontal cortex and hippocampus of T1DCD and CONT mice. (F) Representative immunohistochemical staining of 4-HNE proteins (brown spots, 200×) and corresponding quantitative results in the frontal cortex and hippocampus of T1DCD and CONT mice. Data are presented as mean ± standard error of mean (SEM). The difference between two groups was analyzed using two-tailed unpaired Student's *t*-test. Significant level: *, $p < 0.05$, **, $p < 0.01$, ***, $p < 0.001$. ns, no significant; FC: fold change.

tex and hippocampus (Fig. 5B and 5D). In addition, we found a significantly lower mRNA level of *Sod1* in the hippocampus of T1DCD mice than CONT mice (Fig. 5D), but a downtrend was observed in the frontal cortex (Fig. 5B). The mRNA levels of antioxidants such as *Gcl-1* and *G6pdh* were significantly reduced in the frontal cortex of T1DCD mice (Fig. 5B), but not in the hippocampus (Fig. 5D). Subsequently, we measured the protein levels of 8-hydroxy-2-deoxyguanosine (8-OHdG), a marker of DNA oxidative damage [41], and 4-hydroxynonenal (4-HNE), a marker of oxidative stress-induced lipid peroxidation [42], in these two brain regions of mice by immunohistochemical staining. Fig. 5E demonstrates that the intensity of 8-OHdG-positive staining was significantly higher in the brain of T1DCD than CONT mice, but the frontal cortex ($p < 0.001$, FC = 3.19) had a more pronounced increase than the hippocampal CA1 ($p < 0.001$, FC = 1.78), DG ($p = 0.002$, FC = 1.31) and CA3 ($p = 0.009$, FC = 1.84) regions. Likewise, a significantly higher level of 4-HNE-positive staining was also detected in the brain of T1DCD mice relative to CONT mice, but the frontal cortex ($p < 0.001$, FC = 18.70) showed a higher change rate than the hippocampus (CA1: $p = 0.029$, FC = 6.18; DG: $p = 0.002$, FC = 4.37; CA3: $p = 0.012$, FC = 7.47), as illustrated in Fig. 5F. Collectively, our results suggest that an increase in oxidative stress resulted in cognitive impairment in T1D mice and the frontal cortex might be more vulnerable to oxidative stress than the hippocampus.

The frontal cortex had more pronounced neuroinflammation and neuronal injury than the hippocampus in T1DCD mice

Microglia activation causes oxidative stress and neuroinflammation, contributing to cognitive impairment [43]. Herein we used Iba-1 staining as a microglia marker to quantify the number of activated microglia in the frontal cortex and hippocampus of CONT and T1DCD mice, as illustrated in Fig. 6A. The results reveal that the number of activated microglia was significantly higher in the frontal cortex ($p < 0.001$, FC = 6.76) and hippocampal CA1 ($p = 0.015$, FC = 2.40) and CA3 ($p = 0.016$, FC = 2.01) regions but not DG region ($p > 0.05$, FC = 1.04) of T1DCD mice compared with CONT mice (Fig. 6A). Relative to CONT mice, we detected signifi-

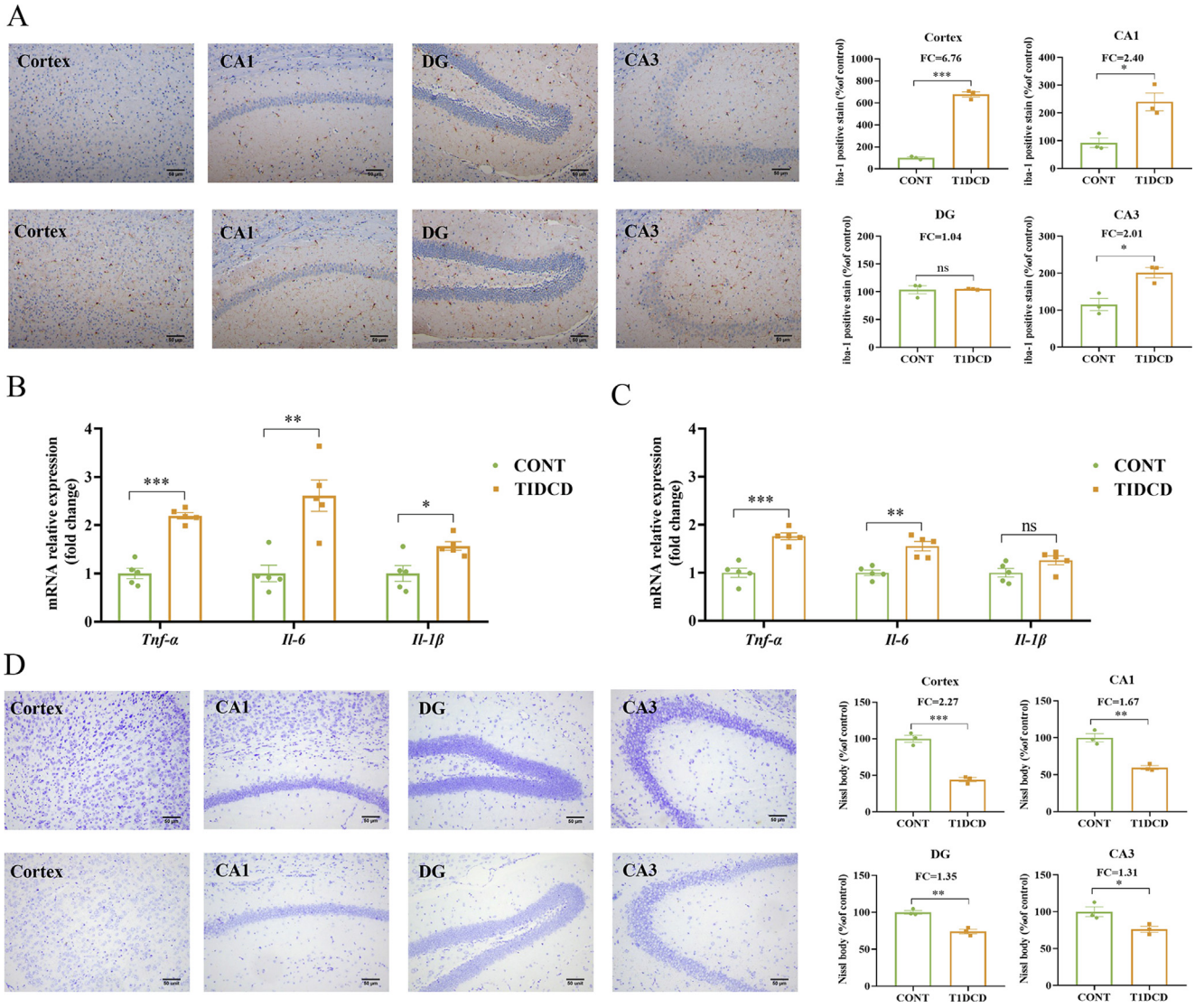

Fig. 6. Brain region-specific changes in neuroinflammation and neuronal injury in type 1 diabetic mice with cognitive decline. (A) Representative immunohistochemical staining of Iba-1 proteins (brown spots, 200×) and corresponding quantitative results in the frontal cortex and hippocampus of type 1 diabetic mice with cognitive decline (T1DCD) and age-matched control mice (CONT). Changes in the mRNA expression levels of proinflammatory cytokines including *Tnf-α*, *Il-6* and *Il-1β* in the (B) frontal cortex and (C) hippocampus between T1DCD and CONT mice. (D) Representative immunohistochemical staining of Nissl body (blue spots, 200×) and corresponding quantitative results in the frontal cortex and hippocampus of T1DCD and CONT. Data are presented as mean ± standard error of mean (SEM). The difference between two groups was analyzed using two-tailed unpaired Student's *t*-test. Significant level: *, $p < 0.05$, **, $p < 0.01$, ***, $p < 0.001$. ns, no significant; FC: fold change.

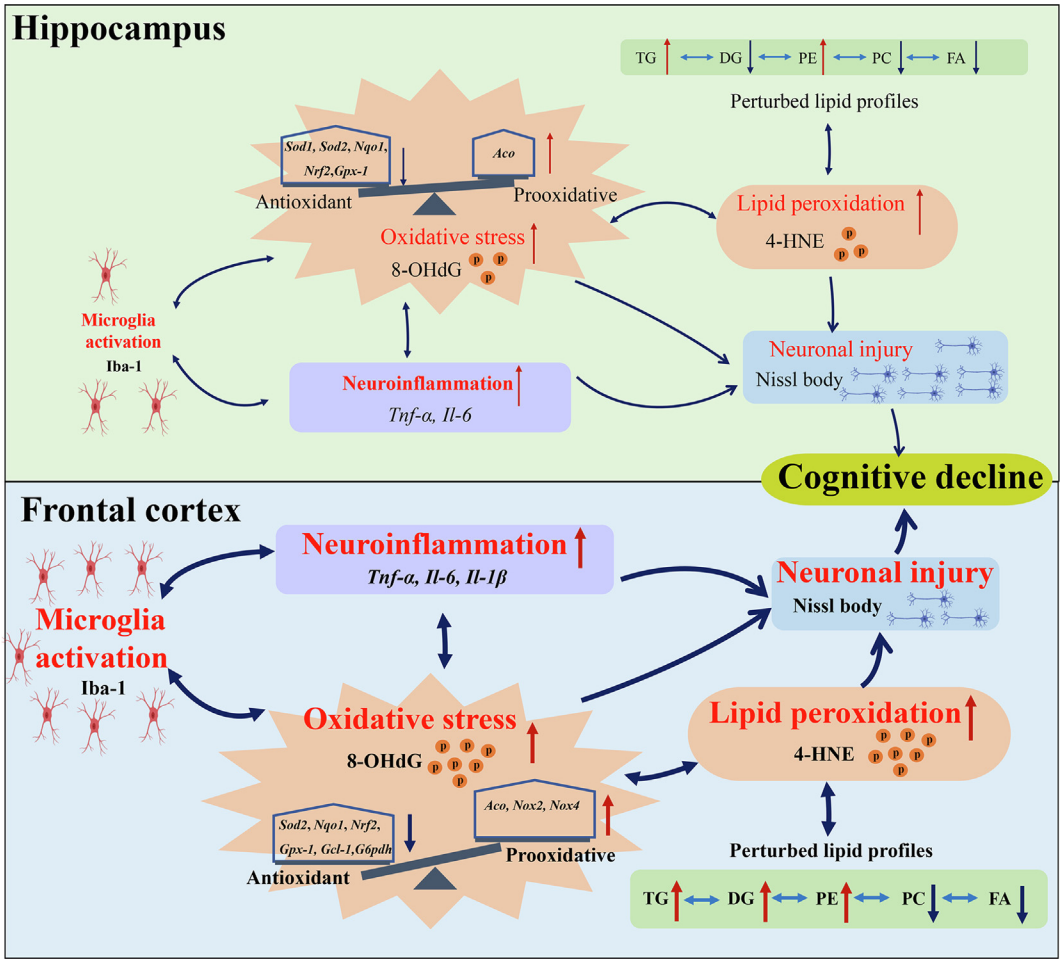

Fig. 7. Schematic diagram of the potential molecular mechanisms underlying diabetic cognitive decline. Under diabetic condition, microglia was activated and then promoted oxidative stress, lipid peroxidation and neuroinflammation, resulting in neuronal injury and cognitive decline, and this phenomenon was more pronounced in the frontal cortex relative to the hippocampus.

cantly increased levels of *Tnf-α* ($p < 0.001$), *Il-6* ($p = 0.002$) and *Il-1β* ($p = 0.015$), as proinflammatory cytokines released from activated microglia, in the frontal cortex of T1DCD mice (Fig. 6B). In the hippocampus, the levels of *Tnf-α* ($p < 0.001$) and *Il-6* ($p = 0.001$) but not *Il-1β* ($p = 0.078$) were also significantly higher in T1DCD mice when compared with CONT mice, as shown in Fig. 6C. Therefore, it should be noting that the frontal cortex had more pronounced inflammatory response than the hippocampus in T1DCD mice. Subsequently, the change in neuronal cells was examined by using Nissl staining in the brain of CONT and T1DCD mice (Fig. 6D). The number of Nissl bodies was significantly decreased in the brain of T1DCD mice relative to CONT mice, but the frontal cortex ($p < 0.001$, FC = 2.27) had a higher reduction than the hippocampus (CA1: $p = 0.003$, FC = 1.67; DG: $p = 0.003$, FC = 1.35; CA3: $p = 0.037$, FC = 1.31), suggesting that more severe neuronal injury occurred in the frontal cortex relative to the hippocampus in T1DCD mice. Collectively, under diabetic condition, microglia was activated and then promoted oxidative stress and neuroinflammation, resulting in neuronal injury and cognitive impairment, and the frontal cortex had a greater impact than the hippocampus (Fig. 7).

Discussion

Brain metabolic disorders have been associated with T1D-induced cognitive decline [19]. In this study, we optimized an integrated analytical method of metabolomics and lipidomics for brain tissue using UPLC-Q-TOF-MS and provided a comprehensive metabolite and lipid profiling in the hippocampal and frontal cortex of T1DCD mice. Based on metabolic pathway analysis, we found that T1DCD mice displayed a higher level of lipid peroxidation in the brain than CONT mice. Lipids are essential ingredients in the cellular membrane that maintains normal structure and function of cells. Thus, excessive lipid oxidation destroys the cellular membrane and leads to cell death [44], which may result in neuronal injury in this study. Of note, moreover, lipid peroxidation is a major influencing factor to oxidative stress [45]. Expectedly, we observed an increased oxidative stress status in the brain of T1DCD mice, which has been considered as one of the major causes of cognitive decline [46]. Microglia as the primary immune cells in the central nervous system closely interplays with oxidative stress [43]. In T1DCD mice, microglia was activated and then induced the release of inflammatory factors *Tnf-α*, *Il-6* and *Il-1β*, resulting in neuroinflammation and neuronal injury. Therefore, our data suggest that microglia-driven oxidative stress and neuroinflammation as the major cause of neurodegenerative diseases [47,48] may also cause T1D-induced cognitive impairment, indicating that diabetes is closely associated with neurodegenerative diseases [49,50]. Another interesting finding in this study is that the frontal cortex exhibited higher levels of microglia activation, oxidative stress and neuroinflammation than the hippocampus in T1DCD mice. Elahi et al. [51] reported that STZ treatment increased oxidative stress and lipid peroxidation in the hippocampus of diabetic mice, but not in the midbrain and cerebellum. Hence, region-specific vulnerability to oxidative stress and neuroinflammation in the diabetic brain

should be considered for the diagnosis, prevention and treatment of diabetic cognitive decline in clinical practice.

Oxidative stress and inflammation are also the major influencing factors for metabolic disorders [52,53]. Herein we found that brain nucleotide metabolism was significantly altered in T1DCD mice, especially in the hippocampus. Nucleotide metabolism serves for maintaining cellular homeostasis due to its essential role in signal transduction, oxidative phosphorylation and nucleotide biosynthesis [54]. Mazumder et al. [55] reported that disturbed purine nucleotide metabolism is a ri6k factor for cognitive dysfunction in patients with chronic kidney disease. Our results suggest that disordered nucleotide metabolism may result in cognitive decline induced by T1D. Energy metabolism has been regarded as both the source and target of oxidant species [56]. In this study, a decrease in energy metabolism was observed in both the frontal cortex and hippocampus of T1DCD mice. Disrupted cerebral energy metabolism has been proved to induce cognitive injury in neurodegenerative diseases such as Alzheimer's disease [57] and Parkinson's disease [58]. Previously, we also revealed that reduced brain energy metabolism may be implicated in diabetic cognitive decline [19,59]. Moreover, oxidative stress also affected cognitive functions via regulating neurotransmitters [60]. Here we observed a disrupted neurotransmitter metabolism in T1DCD mice in a brain region-specific manner. For example, the level of *N*-acetyl-L-aspartate, a neuronal marker, was significantly decreased in both brain regions in T1DCD mice. Moreover, reduced L-dopa, L-aspartate and L-alanine and an increased acetylcholine were found in the hippocampus of T1DCD mice relative to CONT mice, while the levels of aromatic amino acids, as precursors of dopamine and serotonin [61], were significantly lower in the frontal cortex. In our previous study, region-specific shifts in neurotransmitter metabolism were also reported in the brain of both T1D [19] and T2D [10] mice with cognitive dysfunction. Therefore, the present study suggests that oxidative stress and neuroinflammation may promote brain metabolic disorders and cause diabetic cognitive decline.

Conclusion

In this study, an integrated method of metabolomics and lipidomics was optimized for brain tissue using a LC-MS-based analytical platform, and comprehensive metabolite and lipid profiling were provided in the hippocampus and frontal cortex of T1DCD mice. We reveal that the frontal cortex had higher levels of microglia activation, lipid peroxidation, oxidative stress and neuroinflammation than the hippocampus in T1DCD mice. Additionally, T1DCD mice displayed brain metabolic disorders in a region-specific manner. Our results suggest that brain region-specific changes of oxidative stress and neuroinflammation prompt diabetic cognitive decline, but the frontal cortex might be a major target brain region under diabetic condition.

Compliance with Ethics Requirements

All experiments involving animals were conducted according to the ethical policies and procedures approved by the Ethics Committee of Wenzhou Medical University, China (Approval no.: xmsq2021-0502).

CRediT authorship contribution statement

Fen Xiong: Investigation, Methodology, Visualization, Writing – original draft, Writing – review & editing. **Kaiyan Gong:** Investigation, Methodology, Visualization, Writing – review & editing. **Hangying Xu:** Investigation, Methodology, Writing – review & editing. **Yingxin Tu:** Investigation, Writing – review & editing. **Jiahui Lu:** Investigation, Methodology, Writing – review & editing. **Yiyang Zhou:** Investigation, Methodology, Writing – review & editing. **Wenting He:** Investigation, Writing – review & editing. **Wenqing Li:** Investigation, Writing – review & editing. **Chen Li:** Investigation, Writing – review & editing. **Liangcai Zhao:** Investigation, Writing – review & editing. **Hongchang Gao:** Conceptualization, Supervision, Project administration, Funding acquisition, Writing – review & editing. **Hong Zheng:** Conceptualization, Methodology, Investigation, Formal analysis, Resources, Data curation, Visualization, Supervision, Funding acquisition, Writing – original draft, Writing – review & editing.

Declaration of Competing Interest

The authors declare that they have no known competing financial interests or personal relationships that could have appeared to influence the work reported in this paper.

Acknowledgments

This study was supported by the National Natural Science Foundation of China (Approve No.: 22074106, 21974096, and 81771386). The Scientific Research Center of Wenzhou Medical University is acknowledged for technical services.

Appendix A. Supplementary material

Supplementary data to this article can be found online at https://doi.org/10.1016/j.jare.2022.02.011.

References

[1] Katsarou A, Gudbjörnsdottir S, Rawshani A, Dabelea D, Bonifacio E, Anderson BJ, et al. Type 1 diabetes mellitus. Nat Rev Dis Primers 2017;3(1). doi: https://doi.org/10.1038/nrdp.2017.16.
[2] International Diabetes Federation. IDF Diabetes Atlas. 9th ed. Brussels, Belgium: International Diabetes Federation; 2019. http://www.diabetesatlas.org.
[3] Biessels GJ, Whitmer RA. Cognitive dysfunction in diabetes: how to implement emerging guidelines. Diabetologia 2020;63(1):3–9.
[4] Kodl CT, Seaquist ER. Cognitive dysfunction and diabetes mellitus. Endocr Rev 2008;29:494–511.
[5] Li W, Qu Z, Prakash R, Chung C, Ma H, Hoda MN, et al. Comparative analysis of the neurovascular injury and functional outcomes in experimental stroke models in diabetic Goto-Kakizaki rats. Brain Res 2013;1541:106–14.
[6] Hao L, Li Q, Zhao X, Li Y, Zhang Ce. A long noncoding RNA LOC103690121 promotes hippocampus neuronal apoptosis in streptozotocin-induced type 1 diabetes. Neurosci Lett 2019;703:11–8.
[7] Hamed SA. Brain injury with diabetes mellitus: evidence, mechanisms and treatment implications. Expert Rev Clin Pharmacol 2017;10(4):409–28.
[8] Zortul H, Aricioglu F, Hafez G, Yazir Y, Utkan T. Effect of agmatine on impairment of hippocampal neurogenesis and neuroinflammation in streptozotocin-induced diabetes in rats. Eur Neuropsychopharmacol 2019;29:S260–1.
[9] Haskins K, Bradley B, Powers K, Fadok V, Flores S, Ling X, et al. Oxidative stress in type 1 diabetes. Ann N Y Acad Sci 2003;1005(1):43–54.
[10] Zheng H, Zheng Y, Zhao L, Chen M, Bai G, Hu Y, et al. Cognitive decline in type 2 diabetic db/db mice may be associated with brain region-specific metabolic disorders. BBA-Mol Basis Dis 2017;1863(1):266–73.
[11] Gao H, Jiang Q, Ji H, Ning J, Li C, Zheng H. Type 1 diabetes induces cognitive dysfunction in rats associated with alterations of the gut microbiome and metabolomes in serum and hippocampus. BBA-Mol Basis Dis 2019;1865(12):165541. doi: https://doi.org/10.1016/j.bbadis.2019.165541.
[12] Deberardinis RJ, Thompson CB. Cellular metabolism and disease: what do metabolic outliers teach us? Cell 2012;148:1132–44.
[13] Nicholson JK, Lindon JC. Systems biology: Metabonomics. Nature 2008;455(7216):1054–6.
[14] Yanes O, Tautenhahn R, Patti GJ, Siuzdak G. Expanding coverage of the metabolome for global metabolite profiling. Anal Chem 2011;83(6):2152–61.
[15] Wang R, Li B, Lam SM, Shui G. Integration of lipidomics and metabolomics for in-depth understanding of cellular mechanism and disease progression. J Genet Genomics 2020;47(2):69–83.
[16] Yu H, Villanueva N, Bittar T, Arsenault E, Labonté B, Huan T. Parallel metabolomics and lipidomics enables the comprehensive study of mouse

brain regional metabolite and lipid patterns. Anal Chim Acta 2020;1136:168–77.
[17] Mushtaq MY, Choi YH, Verpoorte R, Wilson EG. Extraction for metabolomics: access to the metabolome. Phytochem Anal 2014;25(4):291–306.
[18] Xu X, Zang Q, Zhang R, Liu J, He J, Zhang R, et al. Systematic optimization and evaluation of sample pretreatment methods for LC-MS-based metabolomics analysis of adherent mammalian cancer cells. Anal Methods 2019;11 (23):3014–22.
[19] Xu P, Ning J, Jiang Q, Li C, Yan J, Zhao L, et al. Region-specific metabolic characterization of the type 1 diabetic brain in mice with and without cognitive impairment. Neurochem Int 2021;143:104941. doi: https://doi.org/10.1016/j.neuint.2020.104941.
[20] Lisman J, Buzsáki G, Eichenbaum H, Nadel L, Ranganath C, Redish AD. Viewpoints: how the hippocampus contributes to memory, navigation and cognition. Nat Neurosci 2017;20(11):1434–47.
[21] Badre D, Nee DE. Frontal cortex and the hierarchical control of behavior. Trends Cogn Sci 2018;22(2):170–88.
[22] Paxinos G, Franklin KB. Paxinos and Franklin's the mouse brain in stereotaxic coordinates. Academic Press; 2019.
[23] Wishart DS, Feunang YD, Marcu A, Guo AC, Liang K, Vázquez-Fresno R, et al. HMDB 4.0: the human metabolome database for 2018. Nucleic Acids Res 2018;46:D608–17.
[24] Lin CY, Wu H, Tjeerdema RS, Viant MR. Evaluation of metabolite extraction strategies from tissue samples using NMR metabolomics. Metabolomics 2007;3(1):55–67.
[25] Cubbon S, Antonio C, Wilson J, Thomas-Oates J. Metabolomic applications of HILIC-LC-MS. Mass Spectrom Rev 2010;29(5):671–84.
[26] Tang D-Q, Zou LI, Yin X-X, Ong CN. HILIC-MS for metabolomics: An attractive and complementary approach to RPLC-MS. Mass Spectrom Rev 2016;35 (5):574–600.
[27] López-Bascón MA, Calderón-Santiago M, Díaz-Lozano A, Camargo A, López-Miranda J, Priego-Capote F. Development of a qualitative/quantitative strategy for comprehensive determination of polar lipids by LC–MS/MS in human plasma. Anal Bioanal Chem 2020;412(2):489–98.
[28] Wu H, Southam AD, Hines A, Viant MR. High-throughput tissue extraction protocol for NMR-and MS-based metabolomics. Anal Biochem 2008;372 (2):204–12.
[29] Zheng H, Ni Z, Cai A, Zhang Xi, Chen J, Shu Qi, et al. Balancing metabolome coverage and reproducibility for untargeted NMR-based metabolic profiling in tissue samples through mixture design methods. Anal Bioanal Chem 2018;410 (29):7783–92.
[30] Feng C, Zhu Z, Bai W, Li R, Zheng Yi, Tian X, et al. Proline protects boar sperm against oxidative stress through proline dehydrogenase-mediated metabolism and the amine structure of pyrrolidine. Animals 2020;10(9):1549. doi: https://doi.org/10.3390/ani10091549.
[31] Liang M, Wang Z, Li H, Cai L, Pan J, He H, et al. L-Arginine induces antioxidant response to prevent oxidative stress via stimulation of glutathione synthesis and activation of Nrf2 pathway. Food Chem Toxicol 2018;115:315–28.
[32] Maddineni S, Nichenametla S, Sinha R, Wilson RP, Richie JP. Methionine restriction affects oxidative stress and glutathione-related redox pathways in the rat. Exp Biol Med 2013;238(4):392–9.
[33] Boylan JA, Lawrence KA, Downey JS, Gherardini FC. Borrelia burgdorferi membranes are the primary targets of reactive oxygen species. Mol Microbiol 2008;68(3):786–99.
[34] Overgaard AJ, Weir JM, De Souza DP, Tull D, Haase C, Meikle PJ, et al. Lipidomic and metabolomic characterization of a genetically modified mouse model of the early stages of human type 1 diabetes pathogenesis. Metabolomics 2016;12(1). doi: https://doi.org/10.1007/s11306-015-0889-1.
[35] Park MW, Cha HW, Kim J, Kim JH, Yang H, Yoon S, et al. NOX4 promotes ferroptosis of astrocytes by oxidative stress-induced lipid peroxidation via the impairment of mitochondrial metabolism in Alzheimer's diseases. Redox Biol 2021;41:101947. doi: https://doi.org/10.1016/j.redox.2021.101947.
[36] Sun X, Li X, Jia H, Wang H, Shui G, Qin Y, et al. Nuclear factor E2-related factor 2 mediates oxidative stress-induced lipid accumulation in adipocytes by increasing adipogenesis and decreasing lipolysis. Antioxid Redox Signal 2020;32(3):173–92.
[37] Moldovan O-L, Rusu A, Tanase C, Vari C-E. Glutamate - A multifaceted molecule: Endogenous neurotransmitter, controversial food additive, design compound for anti-cancer drugs. A critical appraisal. Food Chem Toxicol 2021;153:112290. doi: https://doi.org/10.1016/j.fct.2021.112290.
[38] Tiedje KE, Stevens K, Barnes S, Weaver DF. Beta-alanine as a small molecule neurotransmitter. Neurochem Int 2010;57:177–88.
[39] Davison AN, Kaczmarek LK. Taurine-a possible neurotransmitter? Nature 1971;234:107–8.
[40] Frank Henderson J, Paterson ARP. Nucleotide metabolism. Academic Press; 1973.
[41] Graille M, Wild P, Sauvain J-J, Hemmendinger M, Guseva Canu I, Hopf NB. Urinary 8-OHdG as a biomarker for oxidative stress: a systematic literature review and meta-analysis. Int J Mol Sci 2020;21(11):3743. doi: https://doi.org/10.3390/ijms21113743.
[42] Ansari SA, Keshava S, Pendurthi UR, Rao LVM. Oxidative stress product, 4-Hydroxy-2-Nonenal, induces the release of tissue factor-positive microvesicles from perivascular cells into circulation. Arterioscler Thromb Vasc Biol 2021;41:250–65.
[43] Simpson DSA, Oliver PL. ROS generation in microglia: Understanding oxidative stress and inflammation in neurodegenerative disease. Antioxidants 2020;9 (8):743. doi: https://doi.org/10.3390/antiox9080743.
[44] Gaschler MM, Stockwell BR. Lipid peroxidation in cell death. Biochem Biophys Res Commun 2017;482(3):419–25.
[45] Niki E. Lipid peroxidation products as oxidative stress biomarkers. BioFactors 2008;34(2):171–80.
[46] Revel F, Gilbert T, Roche S, Drai J, Blond E, Ecochard R, et al. Influence of oxidative stress biomarkers on cognitive decline. J Alzheimer's Dis 2015;45 (2):553–60.
[47] Hickman S, Izzy S, Sen P, Morsett L, El Khoury J. Microglia in neurodegeneration. Nat Neurosci 2018;21(10):1359–69.
[48] Bartels T, De Schepper S, Hong S. Microglia modulate neurodegeneration in Alzheimer's and Parkinson's diseases. Science 2020;370(6512):66–9.
[49] Biessels GJ, Despa F. Cognitive decline and dementia in diabetes mellitus: mechanisms and clinical implications. Nat Rev Endocrinol 2018;14 (10):591–604.
[50] Farhadi A, Vosough M, Zhang J-S, Tahamtani Y, Shahpasand K. A possible neurodegeneration mechanism triggered by diabetes. Trends Endocrinol Metab 2019;30(10):692–700.
[51] Elahi M, Hasan Z, Motoi Y, Matsumoto S-E, Ishiguro K, Hattori N. Region-specific vulnerability to oxidative stress, neuroinflammation, and tau hyperphosphorylation in experimental diabetes mellitus mice. J Alzheimers Dis 2016;51(4):1209–24.
[52] Rani V, Deep G, Singh RK, Palle K, Yadav UCS. Oxidative stress and metabolic disorders: Pathogenesis and therapeutic strategies. Life Sci 2016;148:183–93.
[53] Hotamisligil GS. Inflammation and metabolic disorders. Nature 2006;444 (7121):860–7.
[54] Lane AN, Fan TW. Regulation of mammalian nucleotide metabolism and biosynthesis. Nucleic Acids Res 2015;43:2466–85.
[55] Mazumder MK, Phukan BC, Bhattacharjee A, Borah A. Disturbed purine nucleotide metabolism in chronic kidney disease is a risk factor for cognitive impairment. Med Hypotheses 2018;111:36–9.
[56] Quijano C, Trujillo M, Castro L, Trostchansky A. Interplay between oxidant species and energy metabolism. Redox Biol 2016;8:28–42.
[57] Kapogiannis D, Mattson MP. Disrupted energy metabolism and neuronal circuit dysfunction in cognitive impairment and Alzheimer's disease. Lancet Neurol 2011;10(2):187–98.
[58] Liu M, Jiao Q, Du X, Bi M, Chen Xi, Jiang H. Potential crosstalk between Parkinson's disease and energy metabolism. Aging Dis 2021;12(8):2003. doi: https://doi.org/10.14336/AD.2021.0422.
[59] Zheng H, Lin Q, Wang D, Xu P, Zhao L, Hu W, et al. NMR-based metabolomics reveals brain region-specific metabolic alterations in streptozotocin-induced diabetic rats with cognitive dysfunction. Metab Brain Dis 2017;32(2):585–93.
[60] Coyle JT, Puttfarcken P. Oxidative stress, glutamate, and neurodegenerative disorders. Science 1993;262(5134):689–95.
[61] Han Q, Phillips RS, Li J. Aromatic amino acid metabolism. Front Mol Biosci 2019;6:22.